Universal rule for the symmetric division of plant cells

Sébastien Besson[1] and Jacques Dumais

Department of Organismic and Evolutionary Biology, Harvard University, The Biological Laboratories, 16 Divinity Avenue, Cambridge, MA 02138

The division of eukaryotic cells involves the assembly of complex cytoskeletal structures to exert the forces required for chromosome segregation and cytokinesis. In plants, empirical evidence suggests that tensional forces within the cytoskeleton cause cells to divide along the plane that minimizes the surface area of the cell plate (Errera's rule) while creating daughter cells of equal size. However, exceptions to Errera's rule cast doubt on whether a broadly applicable rule can be formulated for plant cell division. Here, we show that the selection of the plane of division involves a competition between alternative configurations whose geometries represent local area minima. We find that the probability of observing a particular division configuration increases inversely with its relative area according to an exponential probability distribution known as the Gibbs measure. Moreover, a comparison across land plants and their most recent algal ancestors confirms that the probability distribution is widely conserved and independent of cell shape and size. Using a maximum entropy formulation, we show that this empirical division rule is predicted by the dynamics of the tense cytoskeletal elements that lead to the positioning of the preprophase band. Based on the fact that the division plane is selected from the sole interaction of the cytoskeleton with cell shape, we posit that the new rule represents the default mechanism for plant cell division when internal or external cues are absent.

plant development | mitosis | tissue morphogenesis

The effect of cell shape on spindle orientation and the selection of the division plane in animal and plant cells is a well-documented phenomenon (1–6) first encapsulated in classic 19th century division rules (7, 8). Yet, the nature of the interactions between the mitotic machinery and cell geometry remains for the most part obscure. To shed light on these interactions in plant cells, we revisit a division rule first formulated in 1886 by Léo Errera. Errera's rule states that "the cell plate, at the time of its formation, adopts the geometry that a soap film would take under the same conditions" (9, 10). As is well known, intermolecular forces present within soap films constrain them to adopt configurations that minimize their surface area. Accordingly, Errera's rule is frequently paraphrased as follows: Plant cells divide along the plane of least area that encloses a fix cellular volume (7, 8). In the case of symmetric cell division, the plane of least area is selected such that it creates two daughter cells of equal size, in accordance with another 19th century rule known as Sachs's rule (11, 12). A comparison of the geometry of dividing cells and the equilibrium configurations of soap bubbles placed under the same conditions highlights the predictive power of Errera's rule (Fig. 1) (13). Like soap bubbles, the new wall of recently divided cells conforms to a hallmark feature of area-minimizing surfaces—it meets the cell boundary at 90°, often developing strong curvature to do so (Fig. 1 *A* and *C*). Although the curvature and 90° contact angle of dividing cell walls may seem incompatible with achieving minimal area, these properties arise naturally from a simple geometrical argument (*SI Text* and Fig. S1).

Experimental observations provide a possible mechanistic basis for Errera's rule. In a majority of plant cells, the site of division is first marked by the preprophase band (PPB)—a cytoskeletal
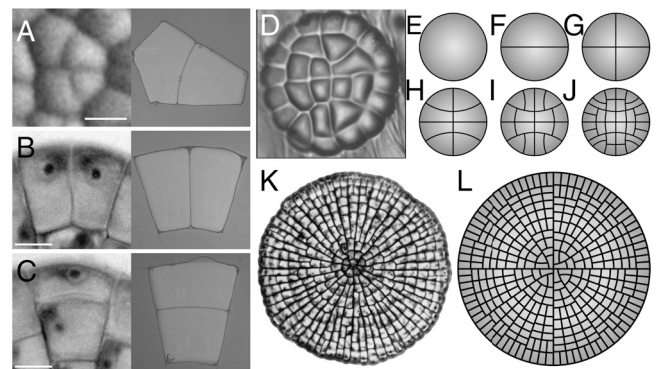

Fig. 1. The division of plant cells and the equilibrium configurations of soap bubbles. (*A–C*) A comparison between dividing cells (*Left*) and the configuration of soap bubbles confined to the same geometry (*Right*). (*A*) *Zinnia elegans*. (*B* and *C*) *Coleochaete orbicularis*. (*D*) Cellular pattern of the glandular trichome of *Dionaea muscipula*. (*E–J*) The development of the trichome is reproduced by successive iterations of Errera's rule for a circular cell growing uniformly over its entire surface. (*K*) Cellular pattern of the thallus of the green alga *Coleochaete orbicularis* (courtesy of P. W. Barlow). (*L*) The development of the thallus is reproduced by successive iterations of Errera's rule for a circular cell with a marginal growth field (see also Movie S1).

structure that forms a closed loop around the cell (14, 15) (Fig. S2). Although the PPB is disassembled before mitosis is completed, its location predicts where the cell plate will fuse with the mother cell wall (10, 16, 17). Given the central role played by the PPB in guiding the cell plate, events leading to its positioning are of particular interest for understanding the selection of the division plane. Observations of premitotic cells have established that cytoplasmic strands populated by microtubules and actin filaments span the space between the nucleus and the cell surface (18–21). Laser-ablation experiments demonstrate that these strands are under tension (22, 23) and are likely responsible for maintaining the nucleus in a central position. The tensional forces would also explain the tendency of the strands to span the shortest distance between the nucleus and the cell surface (21, 24). During preprophase, these strands stabilize cortical microtubules recruited for the PPB and ultimately coalesce into a cytoskeletal structure known as the phragmosome that bridges the nucleus and the cell cortex (18, 19). Because the phragmosome is made of tensile cytoskeletal elements, it naturally converges to a plane of least area. The cytoskeletal dynamics leading to the formation of the phragmosome and PPB may thus explain the surprising similarity observed between dividing cells and the equilibrium configurations of soap bubbles (24).

Even though key elements of a mechanistic basis for Errera's rule were uncovered, the rule faces a seemingly insurmountable challenge; namely, dividing cells provide ample exceptions to discredit any simple generalization one may draw from Errera's soap bubble analogy. Oft-cited examples are the asymmetric divisions that take place during stomatal development (8) and the division of cells in the presence of external cues such as following wounding (25). The most damaging exceptions, however, arise from the failure of Errera's rule to account for the variability observed in symmetric cell divisions, in particular, the fact that cells of identical shape do not necessarily adopt the same division plane. These exceptions strip Errera's rule of most of its predictive power. This work stems from our discovery that a reliable, albeit probabilistic, division rule can be formulated by considering the competition between alternative division planes.

Results

Competing Division Planes in Cells. To probe the competition between alternative division planes, it is convenient to have access to a large population of similarly shaped cells. The quadrant cells of glandular trichomes offer such a system (Fig. 2 *A* and *B*). These cells can divide periclinally and, most frequently, along two anticlinal planes that are mirror images of each other. The breakthrough for this study came from the realization that these division planes are *all* equilibrium configurations for soap bubbles (Fig. 2 *C–E*). To be stable, soap bubble configurations must be local energy minima. For a quadrant shape, the anticlinal configuration has the least energy of all possible configurations (i.e., it is the global minimum), whereas the periclinal division is a local energy minimum. The existence of these alternative energy minima can be demonstrated experimentally by manipulating the interface between the soap bubbles (Fig. 2*F* and Movie S2). In the same fashion, the possible minimal area configurations of plant cells can be computed by exploring the space of all possible division planes (Fig. S3 and Movie S3).

In so far as Errera's rule draws a parallel between dividing plant cells and soap bubbles, the possible coexistence of multiple division planes could have been stated more than 100 years ago. However, what Errera's rule fails to provide is a way to determine how often each of these competing division planes should be observed.

Selection of the Division Plane for Simple Cell Shapes. To investigate how the different division configurations compete as cell shape changes, we focus first on the cells of *Coleochaete* (Fig. 3*A*)
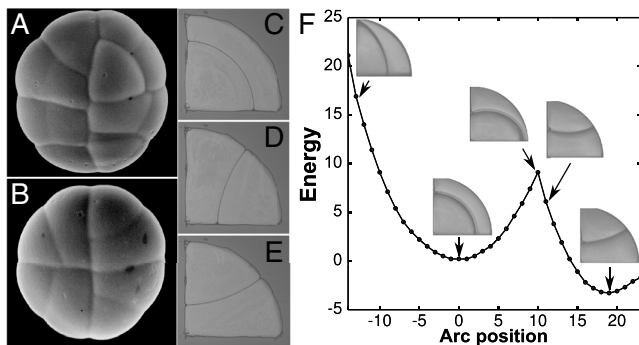

Fig. 2. Alternative division planes for a simple cell shape. (*A* and *B*) Two young glandular trichomes of *Dionaea muscipula*. The glands are made of four nearly identical quadrant cells that can divide according to three different planes—two mirror image anticlinal planes and one periclinal plane. (*C–E*) Equilibrium configurations of soap bubbles reproducing the observed periclinal (*C*) and two anticlinal (*D* and *E*) divisions of the quadrant cells. (*F*) Experimental search of the configuration landscape for two soap bubbles trapped in a circular quadrant. The configurations corresponding to the observed division planes are local area minima, which are also energy minima in the case of soap bubbles (see also Movie S2).

and glandular trichomes (Fig. 3 *B* and *C*) whose simple shapes (trapezoidal and triangular, respectively) can be described with only two parameters (see *Materials and Methods*). These parameters determine the shape of the cell and consequently the limited set of competing division planes. We used this information to define simple shape spaces and to subdivide them into regions where the alternative division planes represent the configuration of least overall area, that is, the global area minimum predicted by Errera's rule (Fig. 3 *A–C*). Cells can be projected in this space based on their shape, and their plane of division can be compared with the predicted configuration.

The shape spaces show clearly the strengths and limitations of Errera's rule. We find that most cells divide as predicted by the global area minimum for their geometry (91%, 66%, and 73%, respectively, for Fig. 3 *A*, *B*, and *C*), and thus conform to Errera's rule. On the other hand, the clustering of "exceptions" around the boundary of domains in shape space (Fig. 3 *A–C*) emphasizes the fundamental problem with a division rule that requires cells to find the division plane of *absolute* minimal area. For cells near the domain boundaries, at least two division planes have very nearly the same surface area. Cells would thus have to measure infinitely small area differences to reliably find the global area minimum. We observe that Errera's rule has high predictive power only for cell shapes that lie far from the domain boundaries and consequently have one division plane with markedly less surface area than other competing planes. A similar conclusion can be drawn from previous work on cell division in plants (26, 27) and animals (2) indicating that alternative division planes become more prominent when the cell's aspect ratio is distinctly in their favor.

These observations can be the basis for a simple postulate—the ability of a cell to distinguish between two alternative division planes is proportional to the area difference between these configurations. For epidermal cells dividing in the plane, the area is equivalent to the length of the division plane. As a measure of the "closeness" of alternative division planes, we can thus adopt the relative length difference $\delta_{ij} = (l_j - l_i)/\rho$, where l_i and l_j are the lengths of two competing configurations (with $l_i < l_j$) and ρ is the mean cell diameter defined as the square root of the cell area. At the domain boundaries, two division planes have exactly the same length so that $\delta_{12} = 0$. As predicted, cells near those boundaries adopt the two alternative division planes with nearly equal probability while one division plane becomes increasingly dominant as the length difference in its favor increases (Fig. 3 *D–F*). Interestingly, the relative length difference also explains the apparent greater variability for the cells of glandular trichomes because the geometry of these cells is such that δ_{12} rarely exceeds 0.15 (Fig. 3 *B* and *C*) compared to >0.5 for *Coleochaete* (Fig. 3*A*).

Selection of the Division Plane in Polygonal Cells. To test the generality of these observations, we look at the apical meristem of *Zinnia elegans* and the leaves of the fern *Microsorum punctatum* (Fig. 4 and Fig. S4). These structures are composed of the characteristic polygonal cells seen in many actively dividing plant tissues. Although the complex cell shape precludes a direct visualization of the shape space, the conclusions stated above still hold. For every cell, we can determine numerically the division planes corresponding to local area minima (Fig. 4 *A–D*). Again, we find that cells more reliably divide along the shortest plane as δ_{12} increases (Fig. 4 *E* and *F*).

A remarkable conclusion lies behind the simple transitions of Fig. 4 *E* and *F*. Unlike the transitions of Fig. 3 *D–F* that map the proportion of two well-defined division planes for graded changes in a basic cell shape, the polygonal cells in these new samples share no common geometrical feature but their value of δ_{12}. This result establishes the relative length difference δ_{ij} as an objective metric for "measuring" the competition between division planes irrespective of cell shape or species.
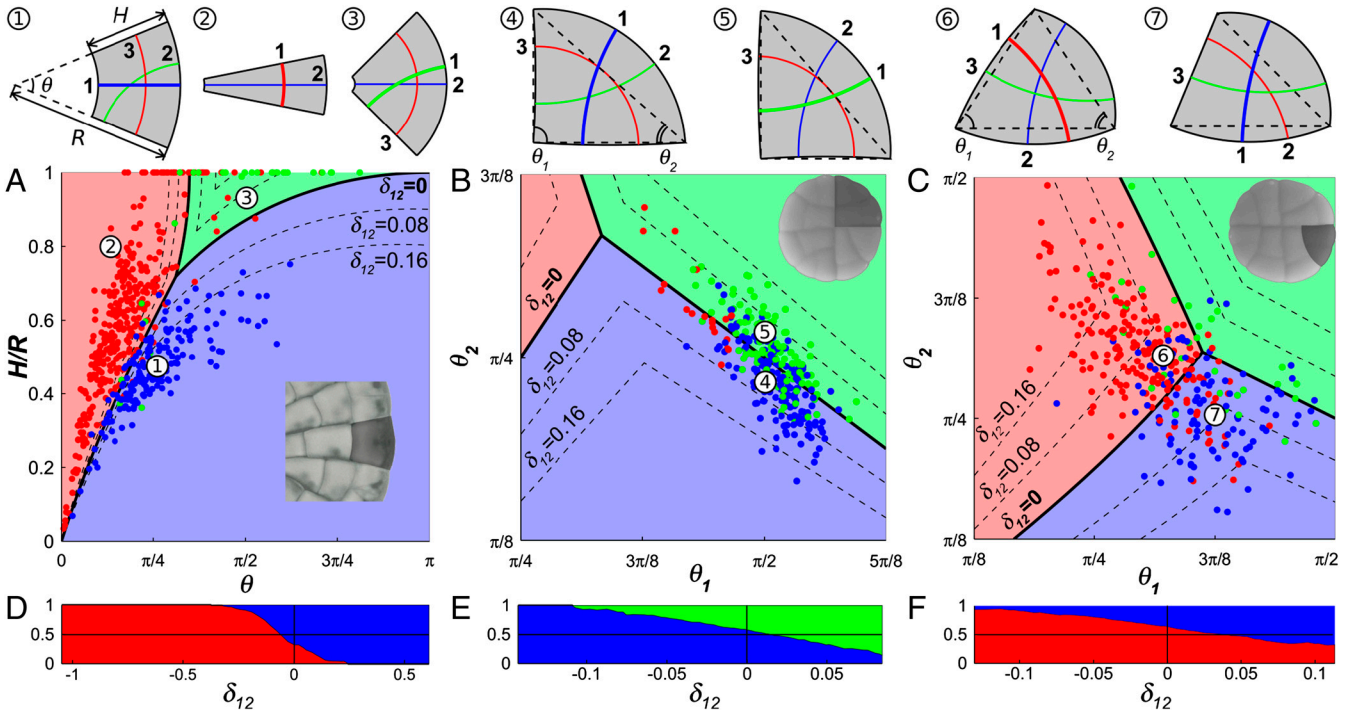
Fig. 3. Selection of the division plane in trapezoidal and triangular cells. (*A–C*) Projection of cells onto the shape spaces for trapezoidal (*A*) and triangular cells (*B* and *C*). The space is divided into domains according to which division plane represents the global area minimum for the location in shape space. The position of each data point is set by the shape of the cell at the time of division and the color of the point indicates the plane of division selected by the cell. Dashed lines are the level curves for different values of δ_{12}. Examples of cell shapes and set of competing division planes are shown at the top of the shape spaces. Division planes are numbered as shortest (1), second shortest (2), etc. (*A*) Projection of 545 trapezoidal cells of *Coleochaete*. (*B*) Projection of 289 quadrant cells of *Dionaea*. (*C*) Projection of 320 triangular cells of *Dionaea*. (*D–F*) Proportion of cells adopting one of two main competing division planes as a function of their relative length difference δ_{12}. The vertical line $\delta_{12} = 0$ corresponds to the domain boundaries in *A* to *C*.

Mechanistic Model of Division. Two important observations emerge from our analysis. First, the plane of division is selected among a small number of area-minimizing configurations (Figs. 3 *A–C* and 4 *A–D*). Second, the probability of a cell adopting a given configuration scales inversely with the relative length or area of the configuration (Figs. 3 *D–F* and 4 *E* and *F*). The known interactions between cytoplasmic strands, their associated microtubules and actin filaments, and cortical microtubules during PPB positioning can explain these two observations. Lloyd and coworkers (21, 24) compared the tense cytoplasmic strands to springs anchoring the nucleus to the cell surface and argued that they must reorganize themselves along a finite number of spatial configurations—each strand connecting the nucleus to an edge by spanning the intervening space with the shortest distance possible (Fig. 5 *A* and *B*). This mechanism offers an elegant explanation for the coexistence of multiple division planes that locally minimize surface area.

We also need to explain how one particular division plane is selected among all possible configurations. Experimental observations indicate that the distribution of strands, or more specifically their associated microtubules, anticipates the position of the PPB; that is, the PPB typically forms on the walls that receive the most endoplasmic microtubules (18, 19, 25) (Fig. 5 *C* and *D*). This raises the question of what determines the number of microtubules connecting to the different cell edges. If s^u is the number of endoplasmic microtubules connecting the nucleus to edge u and S the total number of endoplasmic microtubules, then the microtubule density for edge u is $x^u = s^u/S$. [For clarity we use the following convention: Alternative division planes are identified by the subscripts i,j (as previously), whereas cell edges are identified by the superscripts u,v.] We want to infer the most probable distribution of microtubule densities given some generic constraints on their dynamics. Our approach is based on one tenet supported by experimental observations (28, 29): Microtu-

bules are highly dynamic during the positioning of the PPB. This tenet guarantees that a large number of configurations will be explored as the cell prepares to divide. If so, we would expect the configuration that can be achieved in the greatest number of ways to be the most likely to be observed. This is the central argument for all maximum entropy formulations as used in statistical mechanics and many other systems involving numerous elements in dynamic equilibrium (30).

For a discrete distribution of microtubules on the m sides of a cell, the number of configurations is measured by the Shannon entropy, H:

$$H(x^1 \ldots x^m) = - \sum_{u=1}^{m} x^u \ln(x^u). \qquad [1]$$

Formally, we seek the microtubule distribution maximizing the function $H(x^1 \ldots x^m)$ subject to all the constraints on the system. A first constraint arises from the fact that the relative densities x^u must account for all endoplasmic microtubules and thus must add up to 1:

$$\sum_{u=1}^{m} x^u = 1. \qquad [2]$$

The second constraint encapsulates the idea that the growth of a microtubule can occur only at the expense of others. Evidence that the PPB still forms normally in cells whose de novo protein synthesis is inhibited by drugs (15) suggests that PPB positioning occurs without new tubulin synthesis, but rather results from a reorganization of the existing cytoskeleton. The most direct way to implement this constraint is to stipulate that the average length of microtubules $\langle d \rangle$ is a constant, which we take to be proportional to the mean cell diameter $\rho = \sqrt{A}$. This condition on the cytoskeletal dynamics yields the constraint
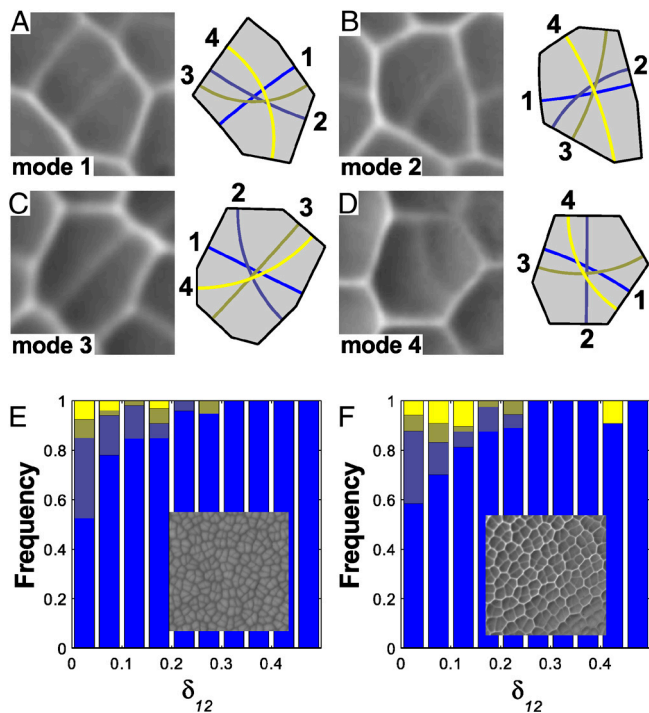
Fig. 4. Selection of the division plane in polygonal cells. (A–D) Replicas of recently divided cells in the leaf of the fern *Microsorum punctatum* (*Left*) and the four shortest division planes predicted for the cell shapes (*Right*). The cells are examples of divisions along the shortest (A), second shortest (B), third shortest (C), and fourth shortest (D) planes. (E) Proportion of different division modes for the shoot apical meristem of *Zinnia elegans*. Overall, 78% of the cells divide along the shortest plane. (*Inset*) Scanning electron micrograph of the shoot apical meristem. (F) Proportion of different division modes for the leaf of the fern *M. punctatum*. Overall, 77% of the cells divide along the shortest plane. (*Inset*) Epoxy replica of the leaf epidermis.

$$\langle d \rangle = \sum_{u=1}^{m} x^u d^u = c\rho, \qquad [3]$$

where d^u is the shortest distance between the nucleus and edge u (i.e., the microtubule length) and c is a constant to be determined experimentally. Maximizing the entropy with these two constraints yields a microtubule distribution $\{x^u\}$ scaling exponentially with the respective lengths d^u:

$$x^u = \frac{e^{-\beta d^u/\rho}}{Z}, \qquad [4]$$

where $Z = \sum_{v=1}^{m} e^{-\beta d^v/\rho}$ is a normalizing factor known as the partition function and β is a parameter to be determined experimentally (see *SI Text* for a complete derivation). We can infer from this distribution that edges flanking the short axis of the cell (i.e., small d^u values) should receive more microtubules. Experimental
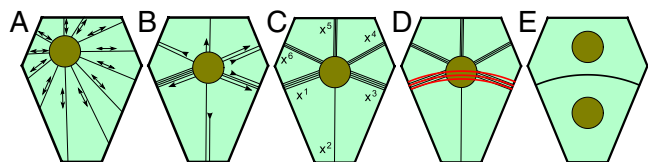

Fig. 5. Mechanistic model for the selection of the division plane. (A) Before preprophase, microtubules radiate from the nucleus. (B) Microtubules reorganize into a finite number of configurations corresponding to the shortest distances between the nucleus and cell edges. (C) The equilibrium configuration favors microtubules that are short. (D) The PPB forms on the edges most heavily populated by microtubules. (E) The cell plate forms at the same position as the PPB. Figure based on refs. 20 and 24.

observations in elongated tobacco BY-2 cells support this conclusion (31, 32).

We must now link this microscopic microtubule distribution to the macroscopic probability of observing a particular division plane. If, as indicated above, the PPB preferentially forms on edges that receive more microtubules, we can infer that the probability that the PPB adjoins the pair of edges 1 and 2 is proportional to the microtubule density on these respective edges:

$$p^{12} = \frac{x^1 x^2}{\sum_{\langle u,v \rangle} x^u x^v}. \qquad [5]$$

Finally, we note that a division configuration i bridging edges u and v will have a length l_i that is very nearly equal to $d^u + d^v$. Using this approximation and Eqs. **4** and **5**, we conclude that the probability of a cell dividing along plane i among N possible configurations follows the relation

$$P_i = p^{uv} = \frac{e^{-\beta l_i/\rho}}{Z}, \qquad [6]$$

where the partition function is now $Z = \sum_{j=1}^{N} e^{-\beta l_j/\rho}$. Relation **6** is known as the Gibbs measure, a probability distribution that arises in many areas of science (30), most notably in statistical mechanics in the form of the Maxwell–Boltzmann distribution (33).

Dividing Cells Follow the Gibbs Measure. To test Eq. **6** and evaluate the parameter β, we first consider the pairwise probability p_{ij} between two competing planes with $l_i < l_j$. In that context, the Gibbs measure can be written as

$$p_{ij} = \frac{P_i}{P_i + P_j} = (1 + e^{-\beta \delta_{ij}})^{-1}, \qquad [7]$$

where δ_{ij} is the relative length difference introduced previously. An analysis that spans the green algae to the angiosperms shows that the proportion of cells dividing along the shortest plane follows precisely this probability distribution with $\beta = 20.6$ (Fig. 6A). With the measured β we test the predictive power of the Gibbs measure by considering the probability of observing the shortest (mode 1) and second shortest (mode 2) configurations against all other possible configurations. We find that our experimental observations support the predicted probabilities for all the systems under consideration (Fig. 6B). These results offer compelling evidence that the equilibrium dynamics of tense cytoskeletal elements explain, in quantitative terms, the positioning of the PPB in symmetrically dividing plant cells.

Discussion

In a seminal paper (24), Lloyd asked how the cytoskeleton reads the geometry of plant cells to align the division plane. He argued that tense cytoplasmic strands rich in microtubules and actin filaments interact with cortical microtubules to guide the PPB and the future plane of division toward a configuration of minimal area. Here, we have developed this idea further by looking at the most likely distribution of tense endoplasmic microtubules given active remodeling of a fixed microtubule pool during preprophase. We have found that such cytoskeletal dynamics would naturally favor microtubules that span the short axis of the cell. This biased microtubule distribution can guide the positioning of the PPB, yielding a precise relation for the probability of alternative division planes. A previously undescribed division rule emerges from these observations: *symmetrically dividing plant cells select a division plane from a set of minimal area configurations according to an exponential probability distribution (the Gibbs measure) that increases inversely with the surface area of the configura-*
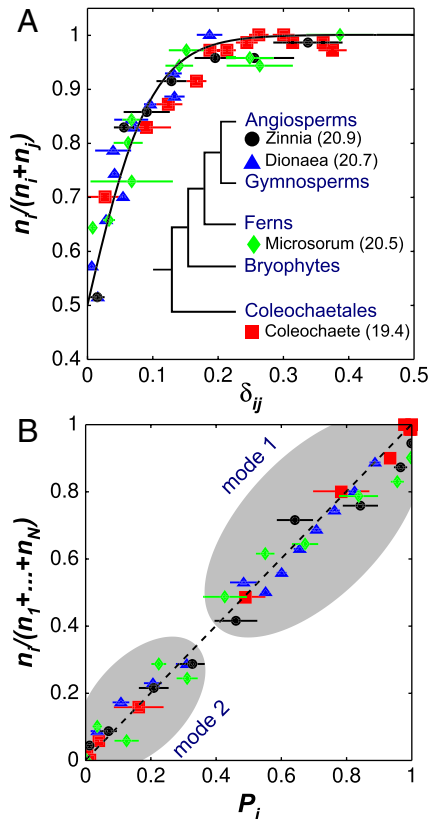
Fig. 6. Universal rule for the selection of the plane of division. (*A*) Proportion of cell divisions along plane i as a function of the relative length difference, δ_{ij}. The proportions are calculated from bins containing at least 70 divisions. The solid line is the best fit of the experimental data with the equation $[1 + e^{-\beta \delta_{ij}}]^{-1}$ and $\beta = 20.6$. Values of β for individual species fits are reported (*Inset*). (*B*) Observed proportion of cell divisions along plane i as a function of the predicted probability $P_i = e^{-\beta l_i / \rho} / Z$. The two clouds correspond to divisions where plane i is the shortest plane (mode 1) and the second shortest plane (mode 2).

tions. For cells dividing in a plane, the rule can be formally restated as follows: plant cells select a division plane i among N competing planes of locally minimal lengths $(l_1, l_2, \ldots, l_i, \ldots, l_N)$ with the probability $P_i = e^{-\beta l_i / \rho} / \sum_j e^{-\beta l_j / \rho}$, where ρ is the square root of the cell area and β is a universal parameter equal to 20.6. We have demonstrated experimentally that this division rule is followed precisely by a wide range of plants.

The direct quantitative link between cytoskeletal dynamics and the observed macroscopic behavior of dividing cells has profound implications on how we view plant cell division. The probability distribution favoring the short axis of the cell is a direct result of the dynamic equilibrium within the pool of endoplasmic microtubules. That asymmetry can emerge within a population of microtubules without the presence of polar cues may at first seem counterintuitive. In the context of our mechanism, cell shape plays the role of cell polarity. Specifically, cell shape gently coaxes endoplasmic microtubules into configurations that favor, but are not limited to, the short axis of the cell. This is an ideal default mechanism for division because the cell does not have to seek actively the configuration of least area. The observed configurations are simply the most probable under the constraints acting on the division machinery. Given the simplicity of the mechanism, we expect the division rule to be observed in most plant cells unless additional cellular controls come into play.

It is of interest to know how the mechanism we have outlined for the symmetric division of plant cells fits in the context of asymmetric cell division, another critical component of developmental

processes in plants. Much work has been devoted to identifying the molecular players controlling this process (34). Although the mechanism of asymmetric division is still not fully elucidated, migration of the nucleus to the polar site appears to be an early conserved feature (35, 36). The final position of the nucleus predicts, in particular, the size ratio of the daughter cells. Although microtubules usually anchor the nucleus to the cell cortex, actin filaments are required for nuclear migration (37). Polar positioning of the nucleus requires an asymmetric distribution of cytoskeletal elements (38) that depends on specific gene products. For example, actin patches involved in eccentric nuclear migration in subsidiary mother cells are regulated by the PAN1 protein (39). A number of other gene products have been shown to be involved in the positioning of the division plane such as the BASL protein in the asymmetric division of the meristemoid mother cell in *Arabidopsis* (40), the PANGLOSS protein in the division of subsidiary mother cells in maize (39, 41), and the POL and PLL1 protein phosphatases in *Arabidopsis* embryos (42). All these genes have the ability to turn cell division into a deterministic process allowing the plant to develop stereotypical cellular patterns. However, the cells of *basl, pan,* and *pol pll1* mutants appear to divide symmetrically (40–42). This result supports the idea that the mechanism we have outlined is the default division mechanism on which polar signals can act to create precise cellular patterns.

Finally, the fact that β is constant for organisms that span 500 million years of evolution raises the question of what this parameter represents. The examination of two limiting regimes provides us with some insights into the physical interpretation of this parameter. At the microscopic level, a large value of β indicates a strong bias of the microtubule population toward the plane of least area. In other words, Errera's rule would be followed perfectly for a very large β-value. On the other hand, for $\beta \ll 1$, the microtubule distribution is uniform across all cell edges and consequently all division planes would be equiprobable. From these limits, we conclude that β is a measure of how responsive the distribution of endoplasmic microtubules is to cell shape. Several molecular players could regulate the outcome of microtubule dynamics. First, a dynamic cytoskeleton is critical to allow the population of microtubules to explore many configurations. Therefore, the magnitude of β may reflect the activity of microtubule-associated proteins and kinases that take part in regulating microtubule dynamics (28). Interestingly, the cytoskeletal reorganization seen during preprophase was indeed shown to be supported by a dramatic increase in the dynamic instability of microtubules both on the cell cortex and in the cytoplasm (28, 29). Another possible factor is the size of the tubulin pool that may affect the strength of the bias favoring short endoplasmic microtubules. These questions will be the focus of future experiments.

Materials and Methods

Tissue Culture and Imaging. Strains of *Coleochaete scutata* and *Coleochaete orbicularis* (LB 2567 and 2651) were obtained from the University of Texas at Austin (UTEX) Culture Collection of Algae. Colonies were grown on 22 × 30 mm coverslips immersed in Bold 3N medium (UTEX). Growth was observed with transmitted light microscopy at 12-h to 24-h time intervals. We used a noninvasive method (43) to produce replicas of leaf trichomes of *Dionaea muscipula* and of the meristem of *Z. elegans*. The replicas were imaged by scanning electron microscopy (FEI Quanta). Finally, epoxy imprints prepared directly from young leaves of *M. punctatum* were observed using light microscopy. Even when sequential material was not available, recent division planes could be identified by their small wall thickness and the T-shaped junctions they formed with the mother cell wall.

Data Acquisition. The cell outlines were extracted from digital images using a computer-assisted routine to position vertices and edges so as to best fit the cells. Cell shapes were approximated by polygons whose edges were straight (*Zinnia* and *Microsorum*) or arcs of circles (*Coleochaete* and *Dionaea*). A class of objects was implemented under Matlab R2007a allowing the systematic

Besson and Dumais

description and analysis of tissues. Each 2D cellular structure was stored as a collection of two-dimensional vertices, edges, and cells. The division planes corresponding to local area minima were computed from analytical solutions when available or through a systematic search of the configuration space (Fig. S3). For *Zinnia* and *Microsorum*, where many configurations compete within a given cell, the division mode was determined using the configuration that minimizes the edge-to-edge Hausdorff distance to the observed division plane (Fig. 4 *A–D*).

Shape Spaces. Projection of the extracted cell outlines onto the shape spaces was achieved using a standard Matlab simplex routine to find the set of parameters minimizing the edge-to-edge Hausdorff distance between the theoretical and extracted cell shapes. For *C. scutata* and *C. orbicularis*, cell shape was modeled as a sector of angle θ on an annulus with inner and outer radii $R - H$ and R, respectively (Fig. 3*A*). These cells can divide along three local minima of length $l_1 = H$, $l_2 = \theta R(1 + (1 - H/R)^2)/2)^{\frac{1}{2}}$, and $l_3 = R(\frac{\pi}{2} - \tau)\tan\tau$, where the angle τ is determined from the condition $(\frac{\pi}{2} - \tau)\tan^2\tau + \tau - \tan\tau = \theta(1 - (1 - H/R)^2)/2$ and satisfies $\tau < \theta$. The cells arising from the third and fourth rounds of division in glandular trichomes of *D. muscipula* were modeled as triangles defined by two angles (θ_1, θ_2). For the quadrant cells, the angle formed by adjacent edges at each vertex was 90° (Fig. 3*B*). For the triangular cells formed by the division of the quadrant cell, the angle at the internal vertex was 90°, but the vertex angles at the gland boundary were equal to 120° due to growth (Fig. 3*C*). For the generic

triangular cells, there is no analytical expression for the lengths of the division planes representing local minima. The shape spaces were thus computed numerically. After identifying the triple point $l_1 = l_2 = l_3$, the boundaries between domains were determined by solving $l_i = l_j$ for every pair (i,j) of division planes. Finally, the different level curves were calculated by solving the equation $\delta_{ij} = (l_j - l_i)/\rho = c$, where c is a preset level.

Division Statistics. The relative proportions reported in Fig. 6 were computed by binning at least 70 divisions based solely on the measured δ_{ij} for the cell or the calculated probability P_i. This approach is "agnostic" in that it does not include the spatial and symmetry information that could be used to label alternative division planes (for example, using the edge of the *Coleochaete* colony to label division planes as anticlinal or periclinal). If a probability is to be attributed to a specific division plane as in Fig. 3 *D–F*, one additional parameter, specific to the system, would have to be added.

1. Bjerknes M (1986) Physical theory of the orientation of astral mitotic spindles. *Science* 234:1413–1416.
2. Strauss B, Adams RJ, Papalopulu N (2006) A default mechanism of spindle orientation based on cell shape is sufficient to generate cell fate diversity in polarised Xenopus blastomeres. *Development* 133:3883–3893.
3. Lintilhac PM, Vesecky TB (1984) Stress-induced alignment of division plane in plant tissues grown in vitro. *Nature* 307:363–364.
4. Yeoman MM, Brown R (1971) Effects of mechanical stress on the plane of cell division in developing callus cultures. *Ann Bot* 35:1102–1112.
5. Théry M, Jiménez-Dalmaroni A, Racine V, Bornens M, Jülicher F (2007) Experimental and theoretical study of mitotic spindle orientation. *Nature* 447:493–496.
6. O'Connell CB, Wang Yl (2000) Mammalian spindle orientation and position respond to changes in cell shape in a dynein-dependent fashion. *Mol Biol Cell* 11:1765–1774.
7. Thompson DW (1942) *On Growth and Form* (Dover, New York).
8. Smith LG (2001) Plant cell division: Building walls in the right places. *Nat Rev Mol Cell Biol* 2:33–39.
9. Errera L (1886) Sur une condition fondamentale d'équilibre des cellules vivantes. [On a fundamental condition of equilibrium for living cells.]. *C R Hebd Seances Acad Sci* 103:822–824 (in French).
10. Wright A, Smith L (2008) Division plane orientation in plant cells. *Cell Division Control in Plants*, eds D Verma and Z Hong (Springer, Berlin), pp 33–57.
11. Sachs J (1878) Über die Anordnung der Zellen in jüngsten Pflanzentheilen [On the arrangement of cells in embryonic tissues]. *Arbeiten des Botanischen Instituts in Würzburg* 2:46–104 (in German).
12. Sachs J (1887) Lecture XXVII. Relations between growth and cell-division in the embryonic tissues. *Lectures in Plant Physiology* (Clarendon Press, Oxford, UK), pp 431–459.
13. Dumais J (2007) Can mechanics control pattern formation in plants? *Curr Opin Plant Biol* 10:58–62.
14. Pickett-Heaps JD, Northcote DH (1966) Organization of microtubules and endoplasmic reticulum during mitosis and cytokinesis in wheat meristems. *J Cell Sci* 1:109–120.
15. Mineyuki Y (1999) The preprophase band of microtubules: Its function as a cytokinetic apparatus in higher plants. *Int Rev Cytol* 187:1–49.
16. Van Damme D (2009) Division plane determination during plant somatic cytokinesis. *Curr Opin Plant Biol* 12:745–751.
17. Müller S, Wright AJ, Smith LG (2009) Division plane control in plants: New players in the band. *Trends Cell Biol* 19:180–188.
18. Wick SM, Duniec J (1983) Immunofluorescence microscopy of tubulin and microtubule arrays in plant cells. I. preprophase band development and concomitant appearance of nuclear envelope-associated tubulin. *J Cell Biol* 97:235–243.
19. Bakhuizen R, van Spronsen PC, Sluiman-den Hertog FAJ, Venverloo CJ, Goosen-de Roo L (1985) Nuclear envelope radiating microtubules in plant cells during interphase mitosis transition. *Protoplasma* 128:43–51.
20. Venverloo CJ, Libbenga KR (1987) Regulation of the plane of cell division in vacuolated cells I: The function of nuclear positioning and phragmosome formation. *J Plant Physiol* 131:267–284.
21. Flanders DJ, Rawlins DJ, Shaw PJ, Lloyd CW (1990) Nucleus-associated microtubules help determine the division plane of plant epidermal cells: Avoidance of four-way junctions and the role of cell geometry. *J Cell Biol* 110:1111–1122.
22. Hahne G, Hoffmann F (1984) The effect of laser microsurgery on cytoplasmic strands and cytoplasmic streaming in isolated plant protoplasts. *Eur J Cell Biol* 33:175–179.
23. Goodbody KC, Venverloo CJ, Lloyd CW (1991) Laser microsurgery demonstrates that cytoplasmic strands anchoring the nucleus across the vacuole of premitotic plant cells are under tension. Implications for division plane alignment. *Development* 113:931–939.
24. Lloyd CW (1991) How does the cytoskeleton read the laws of geometry in aligning the division plane of plant cells? *Development* 113:55–65.
25. Goodbody KC, Lloyd CW (1990) Actin filaments line up across Tradescantia epidermal cells, anticipating wound-induced division planes. *Protoplasma* 157:92–101.
26. Dupuy L, Mackenzie J, Haseloff J (2010) Coordination of plant cell division and expansion in a simple morphogenetic system. *Proc Natl Acad Sci USA* 107:2711–2716.
27. Cooke TJ, Paolillo DJ, Jr (1980) The control of the orientation of cell divisions in fern gametophytes. *Am J Bot* 67:1320–1333.
28. Dhonukshe P, Gadella TWJ (2003) Alteration of microtubule dynamic instability during preprophase band formation revealed by yellow fluorescent protein-CLIP170 microtubule plus-end labeling. *Plant Cell* 15:597–611.
29. Vos JW, Dogterom M, Emons AMC (2004) Microtubules become more dynamic but not shorter during preprophase band formation: A possible "search-and-capture" mechanism for microtubule translocation. *Cell Motil Cytoskel* 57:246–258.
30. Jaynes E, Bretthorst G (2003) *Probability Theory: The Logic of Science* (Cambridge Univ Press, Cambridge, UK).
31. Dhonukshe P, Mathur J, Hulskamp M, Gadella T (2005) Microtubule plus-ends reveal essential links between intracellular polarization and localized modulation of endocytosis during division-plane establishment in plant cells. *BMC Biol* 3:11.
32. Kutsuna N, Hasezawa S (2002) Dynamic organization of vacuolar and microtubule structures during cell cycle progression in synchronized tobacco BY-2 cells. *Plant Cell Physiol* 43:965–973.
33. Schrödinger E (1946) *Statistical Thermodynamics* (Cambridge Univ Press, Cambridge, UK).
34. Abrash EB, Bergmann DC (2009) Asymmetric cell divisions: A view from plant development. *Dev Cell* 16:783–796.
35. Pickett-Heaps JD, Northcote DH (1966) Cell division in the formation of the stomatal complex of the young leaves of wheat. *J Cell Sci* 1:121–128.
36. Kennard JL, Cleary AL (1997) Pre-mitotic nuclear migration in subsidiary mother cells of Tradescantia occurs in G1 of the cell cycle and requires F-actin. *Cell Motil Cytoskeleton* 36:55–67.
37. Cho SO, Wick SM (1990) Distribution and function of actin in the developing stomatal complex of winter rye (Secale cereale cv puma). *Protoplasma* 157:154–164.
38. Panteris E, Apostolakos P, Galatis B (2006) Cytoskeletal asymmetry in Zea mays subsidiary cell mother cells: A monopolar prophase microtubule half-spindle anchors the nucleus to its polar position. *Cell Motil Cytoskel* 63:696–709.
39. Cartwright HN, Humphries JA, Smith LG (2009) PAN1: A receptor-like protein that promotes polarization of an asymmetric cell division in maize. *Science* 323:649–651.
40. Dong J, MacAlister CA, Bergmann DC (2009) BASL controls asymmetric cell division in Arabidopsis. *Cell* 137:1320–1330.
41. Gallagher K, Smith LG (2000) Roles for polarity and nuclear determinants in specifying daughter cell fates after an asymmetric cell division in the maize leaf. *Curr Biol* 10:1229–1232.
42. Song SK, Hofhuis H, Lee MM, Clark SE (2008) Key divisions in the early Arabidopsis embryo require POL and PLL1 phosphatases to establish the root stem cell organizer and vascular axis. *Dev Cell* 15:98–109.
43. Williams MH, Green PB (1988) Sequential scanning electron microscopy of a growing plant meristem. *Protoplasma* 147:77–79.